

# Competitive Photoelectrochemical Methanol and Water Oxidation with Hematite Electrodes

Benjamin Klahr,<sup>§</sup> Sixto Gimenez,<sup>\*,†</sup> Omid Zandi,<sup>‡</sup> Francisco Fabregat-Santiago,<sup>†</sup> and Thomas Hamann<sup>\*,‡</sup>

<sup>§</sup>Department of Chemistry, Northwestern University, 2145 Sheridan Road Evanston, Illinois 60208, United States

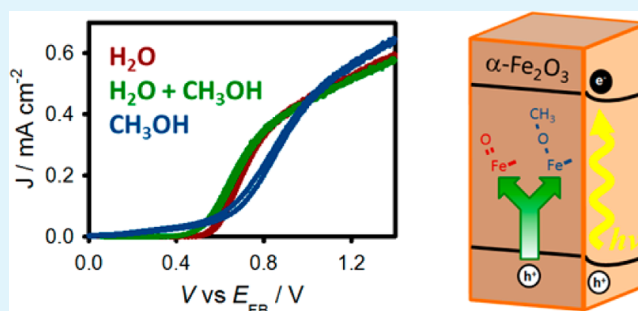
<sup>†</sup>Photovoltaics and Optoelectronic Devices Group, Departament de Física, Universitat Jaume I, 12071 Castelló, Spain

<sup>‡</sup>Department of Chemistry, Michigan State University, 578 South Shaw Lane, East Lansing, Michigan 48824-1322, United States

## S Supporting Information

**ABSTRACT:** Photocatalytic water and methanol oxidation were studied at thin film hematite electrodes synthesized by atomic layer deposition (ALD). Systematic photoelectrochemical characterization along with O<sub>2</sub> evolution measurements were carried out in order to better understand the mechanisms of both water and methanol oxidation at hematite electrodes. When both water and methanol are present in the solution, they are oxidized competitively with each other, allowing the detection and assignment of distinct surface states characteristic to each process. The measurement of different surface states for methanol and water oxidation, along with the absence of measurable surface states in an inert acetonitrile electrolyte, clearly shows that the detected surface states are chemically distinct reaction intermediates of water or methanol oxidation.

**KEYWORDS:** hematite, solar energy, photoelectrocatalysis, water oxidation, methanol oxidation, electrochemical impedance spectroscopy



## INTRODUCTION

Hydrogen derived from solar energy driven water splitting has emerged as one of the most promising candidates to eventually supplant fossil fuels as the chemical fuel of the future, primarily because solar energy and water are essentially inexhaustible, decentralized, and environmentally benign resources.<sup>1</sup> This process can be carried out using a photoelectrochemical cell with semiconductor electrodes immersed in water where the photogenerated electrons and holes are directly used to reduce and oxidize water, respectively.<sup>2</sup> Among the various semiconductor materials tested as photoanodes, hematite ( $\alpha\text{-Fe}_2\text{O}_3$ ) has received a lot of attention due to its combination of sufficiently broad visible light absorption (up to 590 nm), excellent stability under caustic operating conditions, and a valence band positioned sufficiently low to oxidize water.<sup>3,4</sup> Some limitations related to the short collection length of minority carriers have been addressed by nanostructuring, encompassing the orthogonalization of light absorption and minority carrier drift-diffusion directions, as well as alloying strategies.<sup>5–9</sup> Despite recent advances in charge separation, charge collection at the electrode surface has been shown to be a limiting reaction in the overall water splitting process.<sup>10</sup>

In order to boost the efficiency of water splitting photoelectrochemical devices, allowing them to become a viable technology, a detailed understanding of the charge transfer dynamics leading to water oxidation is compulsory. Recent

studies on  $\text{Fe}_2\text{O}_3$  have provided interesting insights into the oxidation mechanisms, recognizing the relevance of surface intermediates for water splitting.<sup>11–14</sup> We recently developed a general physical model, which explicitly includes the existence of a surface state at the semiconductor/liquid interface. This model successfully describes the accumulation of holes at the surface of the semiconductor as an intrinsic part of the water oxidation reaction.<sup>15</sup> When an efficient hole scavenger is placed in the solution, such as  $[\text{Fe}(\text{CN})_6]^{3-/4-}$ , this surface state does not participate in the oxidation process and direct valence band hole transfer to the solution is the dominant oxidation mechanism.<sup>16</sup> Note that this interpretation is not generally accepted, with others suggesting hole trapping at the surface is a process in parallel with direct hole transfer to water.<sup>11,17–19</sup>

Methanol ( $\text{CH}_3\text{OH}$ ) oxidation in the presence of  $\text{H}_2\text{O}$  is a well-studied process, particularly for its relevance for the development of methanol based fuel cells.<sup>20</sup> Methanol has also attracted considerable attention for fundamental studies oriented to the photocatalytic elimination of organic compounds in polluted water and air.<sup>21</sup> Additionally, it has been widely employed as a sacrificial hole scavenger for  $\text{TiO}_2$ ; its oxidation leading to the formation of highly reducing

Received: January 16, 2015

Accepted: March 24, 2015

Published: March 24, 2015

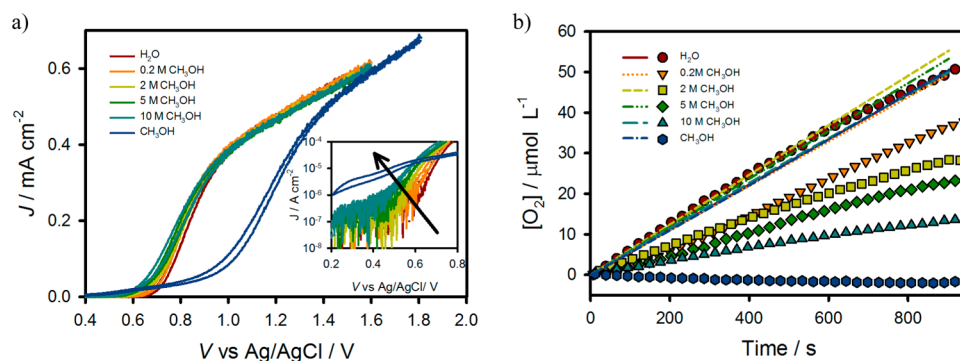


**Figure 1.** (a)  $J$ - $V$  curves of a hematite electrode under 1 sun illumination in contact with  $\text{H}_2\text{O}$  (red), 0.2 M  $\text{CH}_3\text{OH}$  (orange), 2 M  $\text{CH}_3\text{OH}$  (yellow), 5 M  $\text{CH}_3\text{OH}$  (green), 10 M  $\text{CH}_3\text{OH}$  (teal), and  $\text{CH}_3\text{OH}$  (blue) vs Ag/AgCl. (b) Theoretical oxygen produced under 2 sun illumination (lines) and measured  $\text{O}_2$  concentration (shapes) for a hematite electrode in contact with  $\text{H}_2\text{O}$  (solid line and circles), 0.2 M  $\text{CH}_3\text{OH}$  (dotted line and downward pointing triangles), 2 M  $\text{CH}_3\text{OH}$  (short dashed line and squares), 5 M  $\text{CH}_3\text{OH}$  (double dotted dashed line and diamonds), 10 M  $\text{CH}_3\text{OH}$  (long dashed line and upward pointing triangles), and  $\text{CH}_3\text{OH}$  (single dotted line and hexagons). Applied potentials for  $\text{O}_2$  concentration measurements were 1.4 V vs Ag/AgCl for the  $\text{H}_2\text{O}$  and 5 M  $\text{CH}_3\text{OH}$  electrolytes and 1.6 V vs Ag/AgCl for the  $\text{CH}_3\text{OH}$  electrolyte.

hydroxymethyl radicals and consequently to current-doubling.<sup>22</sup> These radicals can further decompose or couple into added value compounds by complex reaction mechanisms<sup>23</sup> and subsequent decomposition can take place by a direct or indirect mechanism.<sup>24–26</sup> In addition, methanol has recently been investigated as a model system of wastewater whose oxidation offers an alternative hydrogen source.<sup>27</sup>

The present study aims to further understand the mechanisms of water and methanol photoinduced oxidation on hematite electrode surfaces. Specifically, the role of a surface state in both media will be resolved, and correlated with the relative rates of water and methanol oxidation. Comparison to an inert acetonitrile electrolyte is also presented which allows confirmation of the assignment of surface states.

## EXPERIMENTAL SECTION

Hematite electrodes (~60 nm thick) were deposited by atomic layer deposition (ALD) and characterized using a previously described procedure.<sup>15</sup> The electrodes were measured in contact with aqueous electrolytes containing a 0.1 M phosphate buffer (pH 6.9) with 0.2 M KCl as supporting electrolyte. This aqueous electrolyte contained varying amounts of methanol ( $\text{CH}_3\text{OH}$ ). Electrolytes containing only methanol as the solvent also contained 0.2 M tetrabutylammonium chloride as supporting electrolyte. The anhydrous methanol and anhydrous acetonitrile solutions were prepared and sealed in an electrochemical cell under nitrogen in a glovebox to minimize the water content. Experiments were also performed with pH 13.6 (1 M KOH) solutions and with different electrodes which all showed the same trends.

Photoelectrochemical and impedance measurements made in aqueous electrolytes were made using a homemade saturated Ag/AgCl reference electrode. Those made in the anhydrous methanol electrolyte were made using a commercial Ag/AgCl electrode (ESA 66-EE009 “no leak”). Both electrodes were calibrated to a saturated calomel electrode (Koslow Scientific) and tested regularly in a  $[\text{Fe}(\text{CN})_6]^{3-/4-}$  solution to ensure consistency. A platinum mesh electrode was used as the counter electrode. Unless noted otherwise, measurements were made under 1 sun illumination (AM 1.5, 100  $\text{mW cm}^{-2}$ ). Cyclic voltammetry (CV) measurements were carried out immediately after the electrode was held at a positive potential (1.6 V vs Ag/AgCl for aqueous electrolytes, 1.8 V vs Ag/AgCl for the methanol electrolyte, and 1.5 V vs Ag/AgCl for acetonitrile electrolyte) and 1 sun illumination for 60 s. This is expected to fully oxidize the surface intermediates. Immediately before scanning the CV, the light is turned off and the CV measurement is made in the dark. For the anhydrous acetonitrile electrolyte, a positive potential of

1.6 V vs Ag/AgCl was applied for 2 h in order to oxidize any trace  $\text{H}_2\text{O}$  in the solution or adsorbed on the electrode surface. Chopped light  $J$ - $V$  curves were measured at a scan rate of 75 mV/s and the light was chopped every 266 ms. The current was sampled at a rate of 500 Hz. Steady state  $J$ - $V$  curves were measured at 20 mV/s. In order to deconvolute the chopped light  $J$ - $V$  curve from potential, constant potential transients were measured after turning the light on (where the anodic current is measured) and turning the light off (where the cathodic current is measured). These transients are labeled the anodic and cathodic transients, respectively. The current was sampled at a rate of 1000 Hz. Impedance measurements were measured at different applied biases using a perturbation amplitude of 10 mV. The frequency range was 10 kHz to 10 mHz. Data were fit using *Zview* software (Scribner Associates). The light source was a 450 W Xe arc lamp (Horiba Jobin Yvon). An AM 1.5 solar filter (Sciencetech Inc.) was used to simulate sunlight at 100  $\text{mW cm}^{-2}$  (1 sun). The pH was determined with a Crison Basic 20 pH meter.

Oxygen measurements were made with an Ocean Optics spectrophotometer using a FOSPOR fluorescent patch. The electrode was illuminated at 2 suns to produce more oxygen and increase the signal-to-noise ratio. The theoretical amount of oxygen produced was calculated by assuming that 4 holes are required to produce 1 molecule of oxygen.

## RESULTS

Figure 1a shows the current density,  $J$ , vs applied voltage,  $V$ , curves of  $\text{Fe}_2\text{O}_3$  in contact with electrolytes with varying concentrations of  $\text{CH}_3\text{OH}$ . When  $\text{CH}_3\text{OH}$  is added to  $\text{H}_2\text{O}$ , a slight cathodic shift of the photocurrent onset takes place (see inset of Figure 1a), in agreement with observations made by other researchers.<sup>11</sup> For anhydrous methanol, however, there is a shallow photocurrent onset observed at a similar potential (0.7 V vs Ag/AgCl), followed by a steeper current onset which mimics the shape measured with water oxidation at hematite electrodes. Surprisingly, there was an anodic shift of approximately 300 mV which was needed to sustain a given photocurrent density of 200  $\mu\text{A cm}^{-2}$  compared to water based electrolytes. This result is in contrast to literature results of hematite photoelectrodes in contact with good hole scavengers, such as  $[\text{Fe}(\text{CN})_6]^{3-/4-}$  and  $\text{H}_2\text{O}_2$ .<sup>28,29</sup>

A fluorescence probe was used to measure the amount of  $\text{O}_2$  produced, which can be used to evaluate the faradaic efficiency of  $\text{H}_2\text{O}$  oxidation. The  $\text{O}_2$  concentration was measured at an applied potential of 1.4 V vs Ag/AgCl for  $\text{H}_2\text{O}$  and  $\text{CH}_3\text{OH}/\text{H}_2\text{O}$  mixture electrolytes and 1.6 V vs Ag/AgCl for the  $\text{CH}_3\text{OH}$  electrolyte such that the photocurrents were

Table 1. Summary of Faradaic Efficiency Due to O<sub>2</sub> Generation for Varying Concentrations of CH<sub>3</sub>OH in H<sub>2</sub>O

[MeOH]/M	[H <sub>2</sub> O]/M	0.75 V vs Ag/AgCl				1.4 V vs Ag/AgCl			
		[O <sub>2</sub> ]/micromoles L <sup>-1</sup>		O <sub>2</sub> faradaic efficiency	relative rate <sup>a</sup>	[O <sub>2</sub> ]/micromoles L <sup>-1</sup>		O <sub>2</sub> faradaic efficiency	relative rate <sup>a</sup>
		theoretical	measured			theoretical	measured		
0.0	55.5	11.17	11.11	99.42%		50.13	49.81	99.36%	
0.2	55.2	7.90	5.41	68.48%	133.48	49.20	36.00	73.17%	106.33
2.0	50.2	12.90	4.01	31.09%	56.52	55.15	28.35	51.40%	24.11
5.0	46.7	10.77	1.89	17.55%	41.35	53.15	22.80	42.90%	11.71
10.0	37.8	7.29	0.59	8.06%	37.65	49.86	15.94	31.97%	7.02

<sup>a</sup>Ratio of CH<sub>3</sub>OH to H<sub>2</sub>O oxidation.

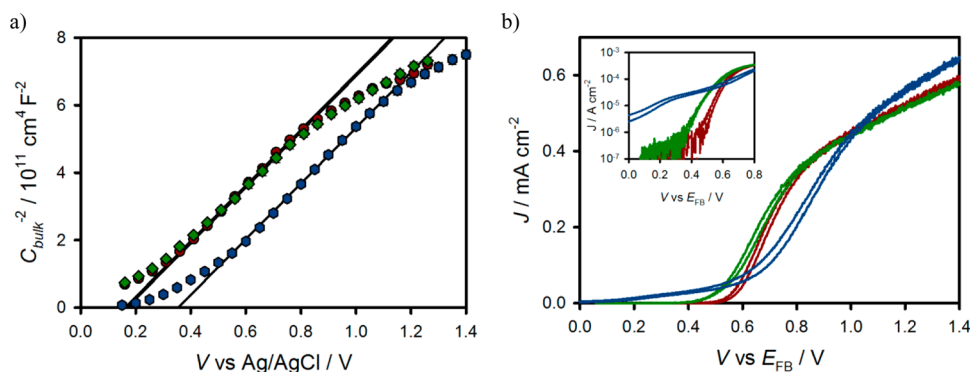


**Figure 2.** (a) Mott–Schottky plot of  $C_{\text{bulk}}$  measured in the dark for H<sub>2</sub>O (red circles), 5 M CH<sub>3</sub>OH (green diamonds), and CH<sub>3</sub>OH electrolytes (blue hexagons). (b)  $J$ – $V$  curves of a hematite electrode under 1 sun illumination in contact with H<sub>2</sub>O (red), 5 M CH<sub>3</sub>OH (green) and CH<sub>3</sub>OH (blue) plotted vs  $E_{\text{FB}}$ .

approximately equal. This potential difference also accounts for the difference in the flat band potential,  $E_{\text{FB}}$ , between aqueous and methanol based electrolytes, *vide infra*. In the case of the aqueous electrolyte, the faradaic efficiency due to O<sub>2</sub> production is approximately unity as shown in Figure 1b and Table 1. As increasing amounts of CH<sub>3</sub>OH are added to H<sub>2</sub>O, the faradaic efficiency due to O<sub>2</sub> generation decreased where no O<sub>2</sub> generation could be detected in anhydrous CH<sub>3</sub>OH. This is expected since the oxidation of CH<sub>3</sub>OH should produce formaldehyde or CO<sub>2</sub>, not O<sub>2</sub>.<sup>25,30,31</sup> Interestingly, a significant amount of O<sub>2</sub> was generated even with large concentrations of CH<sub>3</sub>OH. A summary of the amount of O<sub>2</sub> measured for different CH<sub>3</sub>OH concentrations at applied potentials of 0.75 and 1.4 V vs Ag/AgCl can be seen in Table 1. Assuming that holes oxidize either water to O<sub>2</sub> or methanol to a different product, relative rates,  $\nu_{\text{R}}$ , for CH<sub>3</sub>OH oxidation compared to water oxidation can be calculated by the equation

$$\nu_{\text{R}} = \left( \frac{1 - \text{FE}}{[\text{CH}_3\text{OH}]} \right) \left( \frac{\text{FE}}{[\text{H}_2\text{O}]} \right)^{-1}$$

where FE is the faradaic efficiency for O<sub>2</sub> generation. Results are displayed in Table 1. When considering this relative rate, there is a clear preference for CH<sub>3</sub>OH oxidation compared to H<sub>2</sub>O oxidation, i.e.,  $\nu_{\text{R}}$  is greater than 1 for all potentials and concentrations examined. Despite this preference, the overall rate (current) is not significantly altered by adding CH<sub>3</sub>OH to H<sub>2</sub>O as shown in Figure 1a. Poor current onset potentials still exist with CH<sub>3</sub>OH in solution, showing that it is not acting as a fast and model hole collector as others have suggested.<sup>11</sup>

In order to account for any differences in energetics (band edge movement) due to the different electrolytes, impedance spectroscopy (IS) measurements were performed in the dark. Mott–Schottky plots were generated for pure H<sub>2</sub>O, CH<sub>3</sub>OH

and 5 M CH<sub>3</sub>OH electrolytes by fitting the impedance spectra to a Randle’s circuit. Since the electrode, and therefore dopant density, is the same for all electrolytes, the slope of the Mott–Schottky is expected to be independent of the electrolyte. This is indeed the case, apparent from inspection of Figure 2a. Therefore, to fit the Mott–Schottky plots, the slopes of all 3 electrolytes were fit globally. The extracted dopant density,  $N_{\text{D}}$ , was calculated to be  $5.3 \times 10^{18} \text{ cm}^{-3}$ , in good agreement with previous results.<sup>15,16</sup> The flat band potential was also extracted from the Mott–Schottky plots and can be seen in Table S1. The measured  $E_{\text{FB}}$  for the aqueous electrolytes are nearly equal. In anhydrous CH<sub>3</sub>OH, however, the  $E_{\text{FB}}$  is shifted  $\sim 200$  mV in the positive direction. Part of the difference in  $J$ – $V$  curves can therefore be attributed to a shift in the band energies. In order to carry out an adequate comparison between the different electrolytes, potentials were normalized to their respective  $E_{\text{FB}}$ ’s. Normalized  $J$ – $V$  curves are shown in Figure 2b, which also provide a clear estimate of the overpotentials needed to carry out H<sub>2</sub>O (E) and CH<sub>3</sub>OH oxidation ( $E^\circ = 0.02$  V vs RHE).<sup>20</sup> At high positive applied potentials, the current achieved in all electrolytes is approximately equal; the water oxidation photocurrent has previously been shown to be equal to the current with a fast hole scavenger and controlled only by hole transport to the surface.<sup>16</sup> Thus, we conclude that methanol oxidation with Fe<sub>2</sub>O<sub>3</sub> electrodes does not result in current-doubling reactions. We have suggested previously that in these thin films, at high applied potential, the photocurrent is controlled by the rate of photogenerated holes that reach the surface; i.e., water oxidation is not the rate limiting step. Thus, addition of a fast hole collector (e.g., H<sub>2</sub>O<sub>2</sub> or [Fe(CN)<sub>6</sub>]<sup>4-</sup>) should not increase the current at a given positive Fermi level. Even when correcting for the change in the  $E_{\text{FB}}$ , the steep current onset of anhydrous CH<sub>3</sub>OH oxidation occurs at more

positive potentials compared to H<sub>2</sub>O oxidation suggesting that photoelectrochemical differences cannot be solely attributed to differences in the position of the bands of Fe<sub>2</sub>O<sub>3</sub> in different media.

In order to get more detailed mechanistic information on water and methanol oxidation, impedance spectroscopy measurements were also performed under illumination conditions. Aqueous electrolytes produced Nyquist plots with two clearly distinguishable semicircles near the current onset potential (Supporting Information, Figure S2). A physical model which has been previously developed for the interpretation of charge transfer from hematite electrodes to water can be seen in the form of an equivalent circuit, EC, shown in Figure 3a.<sup>15,16</sup> A graphical representation of this EC

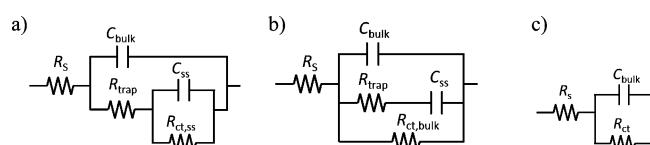


**Figure 3.** (a) Simplified model involving hole transfer through a surface state (b) Simplified model involving direct hole transfer from valence band (c) Randles circuit.

with the physical model of hematite/electrolyte interfaces can be seen in Figure S15. This general model specifically includes the presence of a surface state able to capture conduction band electrons and valence band holes; the trapping-detrapping kinetics are related to  $R_{\text{trap}}$  and the occupancy of the surface state produces a chemical capacitance,  $C_{\text{ss}}$ . Charge transfer takes place through this surface state with a charge transfer resistance,  $R_{\text{ct,ss}}$ . Additionally, a bulk capacitance,  $C_{\text{bulk}}$ , accounts for the space charge capacitance. This EC was used to fit IS data gathered in H<sub>2</sub>O and 5 M CH<sub>3</sub>OH electrolytes. For the pure H<sub>2</sub>O electrolyte, a clear peak in  $C_{\text{ss}}$  develops with voltage which is coincident with the current onset potential (Figure 4a). This peak highlights the requirement for charge accumulation at the surface for water oxidation to occur, and has been pointed out by other researchers.<sup>32–34</sup> When CH<sub>3</sub>OH is added to the aqueous solution, a  $C_{\text{ss}}$  peak is also observed, at the same potential vs  $E_{\text{FB}}$  as shown in Figure 4a. The magnitude of this peak is approximately half that of the H<sub>2</sub>O electrolyte, however, reflecting that fewer holes accumulate at the surface in this state. This result is further corroborated by CV measurements presented below. This result is also in good agreement with the

O<sub>2</sub> evolution measurements displayed in Figure 1b, which indicate that oxidation of both water and methanol leads to the obtained photocurrent. Since the intensity of the  $C_{\text{ss}}$  peak and the rate of O<sub>2</sub> generation are characteristic for water oxidation, the decrease of both measured parameters upon methanol oxidation further indicates that water oxidation occurs through this surface state intermediate. In addition, the decrease of  $C_{\text{ss}}$  upon methanol addition, with a constant photocurrent, clearly shows that water and methanol oxidation are competitive processes, and that methanol oxidation takes place through a different pathway. Despite methanol reducing the measured capacitance of surface states due to water oxidation, two capacitive features are still observed in impedance spectra measured in the anhydrous methanol electrolyte (see the Nyquist plots included as Supporting Information, Figure S2b). Since it appears that charge transfer to methanol occurs through a different pathway than that of water, we invoke another possible EC to describe anhydrous methanol oxidation at hematite electrodes, which is shown in Figure 3b. While both equivalent circuits can be used to fit the CH<sub>3</sub>OH experimental data mathematically, the model in Figure 3b was chosen because its results are corroborated with other techniques including cyclic voltammetry and photocurrent transients, *vide infra*. As in the EC used to describe H<sub>2</sub>O oxidation, this EC still contains a surface state capacitance,  $C_{\text{ss}}$ , and a resistance of transfer to those surface states,  $R_{\text{trap}}$ , based on the observation of two clear semicircles in the Nyquist plot. However, instead of charge transfer through those surface states, this EC contains a separate charge transfer resistance which is not associated with those surface states,  $R_{\text{ct}}$ . This model could imply direct charge transfer from the valence band of the hematite to methanol through an outer-sphere electron transfer mechanism. However, a more likely possibility is that a surface state or surface intermediate is generated, such as a surface adsorbed methoxy species (Fe–O–CH<sub>3</sub>) which is the analogous adsorbed species responsible for methanol oxidation with photogenerated holes on TiO<sub>2</sub>.<sup>30</sup> This mechanism could be interpreted as a single charge transfer resistance if the steady state concentration is very low, resulting in a very low or immeasurable capacitance. By using this model, the obtained trap capacitance shows a double peak feature, with significantly lower intensity compared to that of water based electrolytes (Figure 4a).

Confirmation of the fits can be gained by plotting the total resistance from impedance ( $R_{\text{tot}} = R_s + R_{\text{trap}} + R_{\text{ct,ss}}$  for aqueous electrolytes and  $R_{\text{tot}} = R_s + R_{\text{ct,bulk}}$  for the CH<sub>3</sub>OH electrolyte)

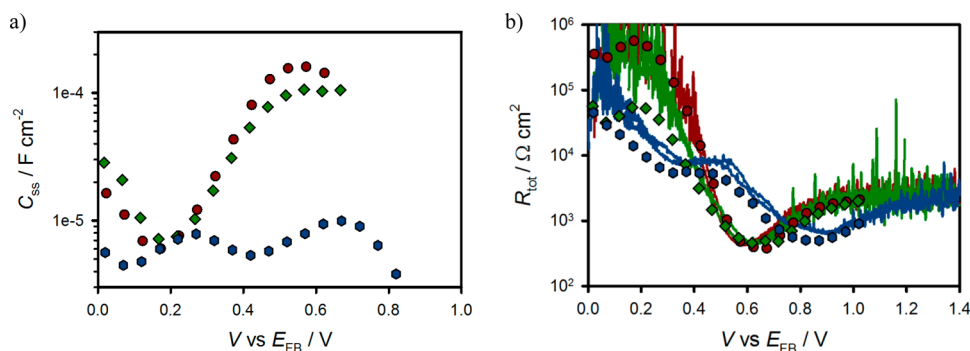


**Figure 4.** (a)  $C_{\text{ss}}$  and (b)  $R_{\text{tot}}$  vs  $E_{\text{FB}}$  extracted from IS analysis under illumination ( $100 \text{ mW}\cdot\text{cm}^{-2}$ ) for a hematite electrode in contact with H<sub>2</sub>O (red circles) 5 M CH<sub>3</sub>OH in H<sub>2</sub>O (green diamonds) and CH<sub>3</sub>OH (blue hexagons). The lines in (b) are obtained by direct derivation of the  $J$ – $V$  curves showed in Figure 2b.

and comparing that to the resistance calculated from the  $J$ - $V$  curves ( $R_{\text{tot}} = dV/dJ$ ). This plot can be seen in Figure 4b. All electrolytes show  $R_{\text{tot}}$  from  $J$ - $V$  curves and  $R_{\text{tot}}$  from IS are in good general agreement indicating that the main resistances which control the  $J$ - $V$  are represented in the impedance spectra. It is interesting to note that anhydrous methanol oxidation involves two different  $R_{\text{tot}}$  dips, around 0.4 V vs  $E_{\text{FB}}$  and 0.8 V vs  $E_{\text{FB}}$ , which appear to be related to the two small  $C_{\text{ss}}$  peaks shown in Figure 4a. This suggests that two different oxidations are being measured: one between 0.2 and 0.6 V vs  $E_{\text{FB}}$  (see Figure 2b) where the slope of the  $J$ - $V$  curve is low, and one above 0.6 V vs  $E_{\text{FB}}$ , where the  $J$ - $V$  curve takes a similar slope as that of aqueous solutions.

The values of the charge transfer resistances ( $R_{\text{ct,ss}}$ ,  $R_{\text{ct,bulk}}$  and  $R_{\text{ct}}$  in Figure 3a,b,c, respectively) and trapping resistances ( $R_{\text{trap}}$ ) derived from the fitted IS spectra are compiled in the Supporting Information, Figure S3. For the aqueous electrolytes where charge transfer is dominated via surface states, and thus fit to the EC in Figure 3a, the relative values of  $R_{\text{trap}}$  and  $R_{\text{ct,ss}}$  depend on the rates of charge transfer, recombination, and a factor determined by the voltage and the trap depth.<sup>35</sup> At low bias (0–0.4 V vs  $E_{\text{FB}}$ ), the addition of  $\text{CH}_3\text{OH}$  to  $\text{H}_2\text{O}$  reduces the charge transfer resistance slightly, but has no effect on the trapping resistance. At these potentials,  $R_{\text{ct,ss}}$  is large and there is no faradaic current (Figure 2b); thus, these values are not directly related to overall water oxidation. The onset potential, which is known to be controlled by surface state recombination,<sup>15</sup> shifts positively in the presence of methanol, indicating that the larger ratio of  $R_{\text{trap}}$  and  $R_{\text{ct,ss}}$  is a result of lower surface state recombination. At potentials positive of the photocurrent onset potential—under water oxidation conditions—the resistances are the same. The values of the  $R_{\text{ct,ss}}$  and  $R_{\text{ct,bulk}}$  derived from fitting the aqueous and methanol solutions, respectively, have different relations to the rates of charge transfer and thus cannot be directly compared.<sup>35</sup> However, the lower  $R_{\text{ct}}$  for methanol oxidation at low bias is consistent with a more negative photocurrent onset potential. At potentials positive of 0.4 V vs  $E_{\text{FB}}$ , the  $R_{\text{ct}}$  values are higher for methanol oxidation, which is consistent with the lower slope of the photocurrent. Finally,  $R_{\text{trap}}$  was found to be higher for anhydrous methanol between 0 and 0.7 V vs  $E_{\text{FB}}$ , consistent with our assignment of hole transfer from the valence band as opposed to trapping.

Cyclic voltammetry experiments were carried out on  $\text{Fe}_2\text{O}_3$  films to measure surface states as previously reported.<sup>16</sup> For these measurements a constant high positive bias (1.6 V vs Ag/AgCl for aqueous electrolytes and 1.8 V vs Ag/AgCl for methanol electrolyte) was initially applied under illumination to fill the surface states with holes. The light was then turned off and a CV was immediately scanned several times (Supporting Information, Figure S4). Cathodic peaks were observed for all electrolytes on the first scan at potentials similar to the potentials where a  $C_{\text{ss}}$  is observed from IS measurements (Figure 5). These peaks are observed at the same energy and with similar relative intensity to those observed in the peaks of  $C_{\text{ss}}$  in Figure 4a. Additional figures including data measured in all  $\text{CH}_3\text{OH}$  electrolytes can be seen in Supporting Information which show the same trend of decreasing cathodic peak currents with the addition of  $\text{CH}_3\text{OH}$ . On the second scan, these peaks disappear because the surface states are not reoxidized at these potentials while in the dark (Supporting Information, Figure S4). The evolution of this peak with scan rate (Supporting Information, Figure S5) also confirms its

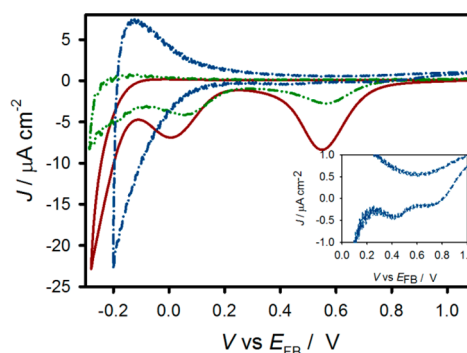


**Figure 5.** Comparison of the first scan of the CV measured at 200 mV/s in  $\text{H}_2\text{O}$  (red solid line), 5 M  $\text{CH}_3\text{OH}$  in  $\text{H}_2\text{O}$  (green double dot dashed line), and  $\text{CH}_3\text{OH}$  (blue single dot dashed line). A magnified image of the  $\text{CH}_3\text{OH}$  curve is shown in the inset which shows 2 small peaks.

capacitive nature.<sup>16</sup> Upon zooming in on the cyclic voltammetry curve for methanol (Figure 5 inset), two small peaks are evident, which is consistent with the  $C_{\text{ss}}$  measured by IS using the model in Figure 3b. It should be noted that these two peaks were not observed in the IS interpretation using the model in Figure 3a (Supporting Information, Figure S7). Thus, these two peaks corroborate the selection of the equivalent circuit for interpreting  $\text{CH}_3\text{OH}$  oxidation at the hematite surface.

The cathodic peak measured at  $\sim 0.55$  V vs  $E_{\text{FB}}$  in the CVs of Figure 5, along with the  $C_{\text{ss}}$  peak observed in IS measurements at the same potential, has been previously attributed to the accumulation of photogenerated holes on the hematite surface in the form of water oxidation intermediates. This peak is always coincident with the water oxidation photocurrent onset and its magnitude is correlated to the water oxidation current; i.e., the peak magnitude is reduced with increasing  $\text{CH}_3\text{OH}$  concentration which competes for photogenerated holes (less water oxidation intermediates form at a given time) (Figure S6). To further show that these capacitive features are a part of the oxidation intermediates of water and methanol, analogous CV measurements were performed in an inert electrolyte, anhydrous acetonitrile, where no hole transfer to solution is expected. The band energy position of the hematite electrode in an acetonitrile electrolyte was controlled through Mott–Schottky measurements, which showed an  $\sim 80$  mV cathodic shift in the flat band potential compared to aqueous electrolytes (Figure S8). Illuminated  $J$ - $V$  curves of a hematite electrode in contact with anhydrous acetonitrile showed negligible background current ensuring the absence of  $\text{H}_2\text{O}$  in the electrolyte (Figure 6a). As shown in Figure 6b for anhydrous acetonitrile solution, no cathodic peaks were observed above the background in the CV measurements suggesting that the cathodic peak observed under  $\text{H}_2\text{O}$  oxidation conditions is specific to  $\text{H}_2\text{O}$  oxidation and not intrinsic to the hematite surface. Interestingly, addition of trace amounts of  $\text{H}_2\text{O}$  to the acetonitrile electrolyte resulted in the development of a cathodic peak in the CV scans, further confirming the assignment of this capacitive feature to species involved in  $\text{H}_2\text{O}$  oxidation reaction (see Supporting Information Figure S8).

The capacitive nature of the surface states of both  $\text{H}_2\text{O}$  and  $\text{CH}_3\text{OH}$  surface states was examined by transient light experiments. Chopped light  $J$ - $V$  curves were obtained and compared to those with constant illumination (Supporting

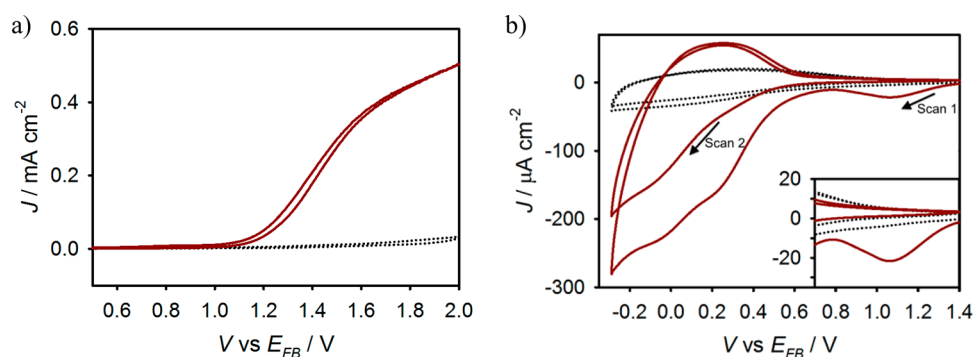


**Figure 6.** (a)  $J$ - $V$  and (b) CV response of a hematite electrode measured in contact with anhydrous MeCN (black dotted line) and after addition of  $10 \mu\text{L H}_2\text{O}$  ( $0.2\%V$ ) to the electrolyte (red solid line).  $J$ - $V$ s were measured under 1 sun illumination and CVs were recorded at  $500 \text{ mV/s}$  in the dark after holding the electrode at  $1.5 \text{ V vs Ag/AgCl}$  under 1 sun illumination for 60 s.

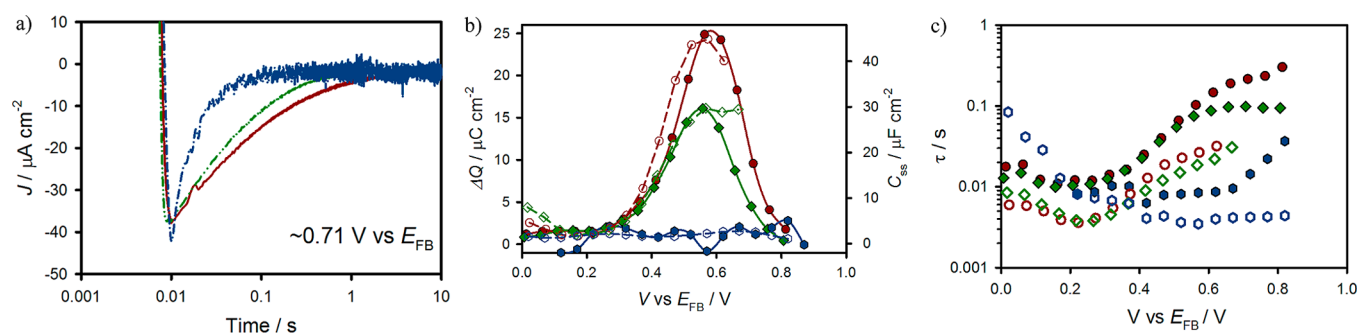


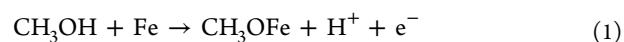
**Figure 7.** (a) Cathodic transients in  $\text{H}_2\text{O}$  (red solid line),  $5 \text{ M CH}_3\text{OH}$  in  $\text{H}_2\text{O}$  (green double dot dashed line), and  $\text{CH}_3\text{OH}$  (blue single dot dashed line) measured within  $5 \text{ mV}$  of  $0.71 \text{ V vs } E_{\text{FB}}$ . (b) The calculated charge passed measured by integrating cathodic transients (filled symbols, solid lines) along with  $C_{\text{ss}}$  measured by IS (hollow symbols, dashed lines) for a hematite electrode in contact with  $\text{H}_2\text{O}$  (red circles),  $5 \text{ M CH}_3\text{OH}$  in  $\text{H}_2\text{O}$  (green diamonds), and  $\text{CH}_3\text{OH}$  (blue hexagons). (c) Lifetimes of transients fit by a single exponential decay (solid shapes) and by multiplying  $C_{\text{ss}}$  and  $R_{\text{trap}}$  (open shapes) for  $\text{H}_2\text{O}$  (red circles),  $5 \text{ M CH}_3\text{OH}$  (green diamonds), and  $\text{CH}_3\text{OH}$  (blue hexagons).

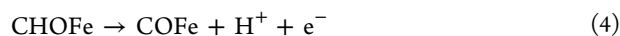
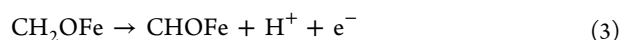
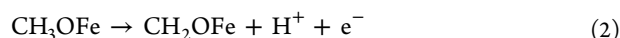
Information, Figure S9). In all tested electrolytes, the presence of anodic and cathodic transients indicated the presence of surface states.<sup>28,36,37</sup> These spikes were analyzed quantitatively by switching the light on (anodic) and off (cathodic) at a constant potential while measuring the current as a function of time. Examples of current transients can be seen in Figure 7a and in Supporting Information, Figures S10–S13. Integration of the cathodic current provides a quantitative measurement of the light-induced charge stored in the surface states, which is shown in Figure 7b, and compared to  $C_{\text{ss}}$  measured by IS. The good agreement between the integrated charge from transient measurements with  $C_{\text{ss}}$  from IS shows that these two measurements are probing the same species.

Single exponential lifetimes of the cathodic transients were calculated and can be seen in Figure 7c. The lifetimes are approximately equal for  $\text{H}_2\text{O}$  and  $5 \text{ M CH}_3\text{OH}$  electrolytes throughout the potential range with the exception of potentials greater than  $\sim 0.6 \text{ V vs } E_{\text{FB}}$  where the mixture has lower lifetimes. These decays are attributed to electrons from the conduction band reducing the oxidized surface states. Since the dominant surface state is related to water oxidation, it is not surprising that these measured lifetimes are constant for the two aqueous electrolytes. We note that this result disagrees with Cowan et al., who showed a decrease in lifetime for a  $10\% \text{ CH}_3\text{OH}$  in  $\text{H}_2\text{O}$  solution compared to a  $\text{H}_2\text{O}$  solution under no applied bias.<sup>38</sup> It is possible, however, that the techniques of transient electrochemistry employed herein and transient absorption spectroscopy employed by Cowan et al. are measuring different species. In the  $\text{CH}_3\text{OH}$  electrolyte, the

lifetimes of these transients are approximately an order of magnitude lower than those measured in aqueous electrolytes at potentials where photocurrent is measured. This is attributed to an increased rate of recombination to surface  $\text{CH}_3\text{OH}$  oxidation intermediates compared to surface  $\text{H}_2\text{O}$  oxidation intermediates.<sup>25</sup> The lifetimes were also calculated by multiplying the  $C_{\text{ss}}$  and  $R_{\text{trap}}$  from IS results and are shown in Figure 7c as open shapes. The same general trend is observed between the lifetimes calculated from transient and EIS measurements.

From the double peak feature observed for  $C_{\text{ss}}$  from IS analysis of anhydrous methanol oxidation, correlated to respective cathodic peaks in the cyclic voltammetry, and dips in the charge transfer resistance ( $R_{\text{ct}}$ ) and total resistance ( $R_{\text{tot}}$ ), it appears that two surface intermediates are being measured during  $\text{CH}_3\text{OH}$  oxidation. A recent paper by Baltrusaitis et al. discusses methanol oxidation on hematite surfaces using theoretical calculations for several surface terminations.<sup>27</sup> Since the electrochemical response of the oxidation of  $\text{H}_2\text{O}$ – $\text{CH}_3\text{OH}$  mixtures is dominated by the redox properties of water surface intermediates (which has been previously discussed in detail),<sup>15,16</sup> this discussion will focus on the oxidation of the anhydrous  $\text{CH}_3\text{OH}$  solution. For the  $\text{Fe-O}_3\text{-R}$  termination of the (0001) surface of hematite (which is the most stable termination under nonaqueous conditions),<sup>39</sup> anhydrous methanol oxidation at the Fe atom is expected to occur as follows:<sup>27</sup>





Under photoelectrochemical conditions (where photogenerated holes are at the valence band potential), steps 1–4 are calculated to be thermodynamically downhill.<sup>27</sup> While these reactions are thermodynamically favored, insight into the rates cannot be easily determined due to the conflation with electron recombination from electrons in the conduction band to the various surface bound species. The two capacitance peaks observed in IS and cyclic voltammetry likely represent potentials where a relatively large concentration of surface bound intermediates form due to a balancing of oxidation of holes from the valence band and recombination from electrons in the conduction band. The identity of these two electrochemically observable species is uncertain, although we speculate that each peak is an independent surface species represented in one of the eqs 1–4. In situ spectroelectrochemistry has recently been used to examine the identity of water oxidation intermediates at the hematite surface, and could also be employed to study methanol oxidation.<sup>17,40</sup> In this manner, the precise molecular details of this mechanism are currently being investigated in our lab.

Finally, concomitant water oxidation is required to produce  $\text{O}^*$  and complete the oxidation of CO to  $\text{CO}_2$ .<sup>27</sup> Since this favored mechanism cannot occur in the anhydrous methanol electrolyte, this explains the very low initial photocurrent densities observed for this electrolyte. Further, in the presence of water, the overall methanol oxidation cannot proceed faster than the water oxidation reaction required to produce  $\text{O}^*$ ; this explains why the addition of methanol does not have a significant effect on the  $J$ – $V$  response of methanol–water mixtures, i.e., water oxidation is the rate-limiting step.

## CONCLUSIONS

The photooxidation of methanol and water was examined at the surface of model hematite photoanodes synthesized by atomic layer deposition (ALD). A surface capacitance correlated with water oxidation is decreased with the addition of  $\text{CH}_3\text{OH}$ . This reduction in surface states, measured by IS, CV, and transient measurements, combined with corroborating  $\text{O}_2$  evolution, further confirms that the surface states are actively participating in the hole transfer mechanism to  $\text{H}_2\text{O}$ , as suggested in previous studies.<sup>15,16</sup> The fact that distinct surface states are measured in anhydrous methanol solutions, and no surface states are measured in an inert anhydrous acetonitrile solution, further proves this point.

## ASSOCIATED CONTENT

### Supporting Information

Additional cyclic voltammograms, EIS fit results, and transient photocurrent measurements. This material is available free of charge via the Internet at <http://pubs.acs.org>.

## AUTHOR INFORMATION

### Corresponding Authors

\*E-mail: [sjulia@fca.uji.es](mailto:sjulia@fca.uji.es).

\*E-mail: [hamann@chemistry.msu.edu](mailto:hamann@chemistry.msu.edu).

### Notes

The authors declare no competing financial interest.

## ACKNOWLEDGMENTS

T.W.H. thanks the National Science Foundation (CHE-1150378) for support of this research. F.F.S. acknowledges support by projects from Ministerio de Ciencia e Innovación (MICINN) of Spain (Consolider HOPE CSD2007-00007), Generalitat Valenciana (PROMETEO/2009/058 and the “Institute of Nanotechnologies for Clean Energies”, under project ISIC/2012/008). F.F.S. thanks the funding of University Jaume I- Bancaixa (Grant P1-1B2011-50).

## REFERENCES

- (1) Lewis, N. S.; Crabtree, G., Eds. *Basic Research Needs for Solar Energy Utilization*; Office of Science, U.S. Department of Energy: Washington, DC, 2005.
- (2) van de Krol, R.; Liang, Y.; Schoonman, J. Solar Hydrogen Production with Nanostructured Metal Oxides. *J. Mater. Chem.* **2008**, *18*, 2311–2320.
- (3) Sivula, K.; Le Formal, F.; Graetzel, M., Solar Water Splitting: Progress Using Hematite ( $\alpha\text{-Fe}_2\text{O}_3$ ) Photoelectrodes. *ChemSusChem* **2011**, *4*, 432–449.
- (4) Lin, Y.; Yuan, G.; Sheehan, S.; Zhou, S.; Wang, D. Hematite-based Solar Water Splitting. *Challenges and Opportunities* **2011**, *4*, 4862–4869.
- (5) Brillet, J.; Gratzel, M.; Sivula, K. Decoupling Feature Size and Functionality in Solution-Processed, Porous Hematite Electrodes for Solar Water Splitting. *Nano Lett.* **2010**, *10*, 4155–4160.
- (6) Lin, Y.; Zhou, S.; Sheehan, S. W.; Wang, D. Nanonet-Based Hematite Heteronanostructures for Efficient Solar Water Splitting. *J. Am. Chem. Soc.* **2011**, *133*, 2398–2401.
- (7) Sivula, K.; Zboril, R.; Le Formal, F.; Robert, R.; Weidenkaff, A.; Tucek, J.; Frydrych, J.; Graetzel, M. Photoelectrochemical Water Splitting with Mesoporous Hematite Prepared by a Solution-Based Colloidal Approach. *J. Am. Chem. Soc.* **2011**, *132*, 7436–7444.
- (8) Steier, L.; Herraiz-Cardona, I.; Gimenez, S.; Fabregat-Santiago, F.; Bisquert, J.; Tilley, S. D.; Grätzel, M. Understanding the Role of Underlayers and Overlayers in Thin Film Hematite Photoanodes. *Adv. Funct. Mater.* **2014**, *24*, 7681–7688.
- (9) Zandi, O.; Klahr, B. M.; Hamann, T. W. Highly Photoactive Ti-doped  $\alpha\text{-Fe}_2\text{O}_3$  Thin Film Electrodes: Resurrection of the Dead Layer. *Energy Environ. Sci.* **2013**, *6*, 634–642.
- (10) Young, K. M. H.; Klahr, B. M.; Zandi, O.; Hamann, T. W. Photocatalytic Water Oxidation with Hematite Electrodes. *Catal. Sci. Technol.* **2013**, *3*, 1660–1671.
- (11) Pendlebury, S. R.; Barroso, M.; Cowan, A. J.; Sivula, K.; Tang, J. W.; Gratzel, M.; Klug, D.; Durrant, J. R. Dynamics of Photogenerated Holes in Nanocrystalline  $\alpha\text{-Fe}_2\text{O}_3$  Electrodes for Water Oxidation Probed by Transient Absorption Spectroscopy. *Chem. Commun.* **2011**, *47*, 716–718.
- (12) Pendlebury, S. R.; Cowan, A. J.; Barroso, M.; Sivula, K.; Ye, J.; Gratzel, M.; Klug, D. R.; Tang, J.; Durrant, J. R. Correlating Long-Lived Photogenerated Hole Populations with Photocurrent Densities in Hematite Water Oxidation Photoanodes. *Energy Environ. Sci.* **2012**, *5*, 6304–6312.
- (13) Peter, L. M.; Wijayantha, K. G. U.; Tahir, A. A. Kinetics of Light-Driven Oxygen Evolution at  $\alpha\text{-Fe}_2\text{O}_3$  Electrodes. *Faraday Discuss.* **2012**, *155*, 309–322.
- (14) Upul Wijayantha, K. G.; Saremi-Yarahmadi, S.; Peter, L. M. Kinetics of Oxygen Evolution at  $\alpha\text{-Fe}_2\text{O}_3$  Photoanodes: A Study by Photoelectrochemical Impedance Spectroscopy. *Phys. Chem. Chem. Phys.* **2011**, *13*, 5264–5270.
- (15) Klahr, B.; Gimenez, S.; Fabregat-Santiago, F.; Hamann, T.; Bisquert, J. Water Oxidation at Hematite Photoelectrodes: The Role of Surface States. *J. Am. Chem. Soc.* **2012**, *134*, 4294–4302.
- (16) Klahr, B.; Gimenez, S.; Fabregat-Santiago, F.; Bisquert, J.; Hamann, T. Electrochemical and Photoelectrochemical Investigation of Water Oxidation with Hematite Electrodes. *Energy Environ. Sci.* **2012**, *5*, 7626–7636.

- (17) Barroso, M.; Pendlebury, S. R.; Cowan, A. J.; Durrant, J. R. Charge Carrier Trapping, Recombination and Transfer in Hematite ( $\alpha\text{-Fe}_2\text{O}_3$ ) Water Splitting Photoanodes. *Chem. Sci.* **2013**, *4*, 2724–2734.
- (18) Barroso, M.; Cowan, A. J.; Pendlebury, S. R.; Grätzel, M.; Klug, D. R.; Durrant, J. R. The Role of Cobalt Phosphate in Enhancing the Photocatalytic Activity of  $\alpha\text{-Fe}_2\text{O}_3$  Toward Water Oxidation. *J. Am. Chem. Soc.* **2011**, *133*, 14868–14871.
- (19) Barroso, M.; Mesa, C. A.; Pendlebury, S. R.; Cowan, A. J.; Hisatomi, T.; Sivula, K.; Grätzel, M.; Klug, D. R.; Durrant, J. R. Dynamics of Photogenerated Holes in Surface Modified  $\alpha\text{-Fe}_2\text{O}_3$  Photoanodes for Solar Water Splitting. *Proc. Natl. Acad. Sci. U.S.A.* **2012**, *109*, 15640–15645.
- (20) Iwasita, T. Electrochemical Oxidation of Methanol. *Electrochim. Acta* **2002**, *47*, 3663–3674.
- (21) Hoffmann, M. R.; Martin, S. T.; Choi, W.; Bahnemann, D. W. Environmental Applications of Semiconductor Photocatalysis. *Chem. Rev.* **1995**, *95*, 69–96.
- (22) Kho, Y. K.; Iwase, A.; Teoh, W. Y.; Madler, L.; Kudo, A.; Amal, R. Photocatalytic  $\text{H}_2$  Evolution over  $\text{TiO}_2$  Nanoparticles. The Synergistic Effect of Anatase and Rutile. *J. Phys. Chem. C* **2010**, *114*, 2821–2829.
- (23) Lu, H.; Zhao, J.; Li, L.; Gong, L.; Zheng, J.; Zhang, L.; Wang, Z.; Zhang, J.; Zhu, Z. Selective Oxidation of Sacrificial Ethanol Over  $\text{TiO}_2$ -Based Photocatalysts During Water Splitting. *Energy Environ. Sci.* **2011**, *4*, 3384–3388.
- (24) Chen, J.; Ollis, D. F.; Rulkens, W. H.; Bruning, H. Photocatalyzed Oxidation of Alcohols and Organochlorides in the Presence of Native  $\text{TiO}_2$  and Metallized  $\text{TiO}_2$  Suspensions. Part (II): Photocatalytic Mechanisms. *Water Resour.* **1999**, *33*, 669–676.
- (25) Villarreal, T. L.; Gómez, R.; Neumann-Spallart, M.; Alonso-Vante, N.; Salvador, P. Semiconductor Photooxidation of Pollutants Dissolved in Water: A Kinetic Model for Distinguishing between Direct and Indirect Interfacial Hole Transfer. I. Photoelectrochemical Experiments with Polycrystalline Anatase Electrodes under Current Doubling and Absence of Recombination. *J. Phys. Chem. B* **2004**, *108*, 15172–15181.
- (26) Mora-Seró, I.; Villarreal, T. L.; Bisquert, J.; Pitarch, Á.; Gómez, R.; Salvador, P. Photoelectrochemical Behavior of Nanostructured  $\text{TiO}_2$  Thin-Film Electrodes in Contact with Aqueous Electrolytes Containing Dissolved Pollutants: A Model for Distinguishing between Direct and Indirect Interfacial Hole Transfer from Photocurrent Measurements. *J. Phys. Chem. B* **2005**, *109*, 3371–3380.
- (27) Baltrusaitis, J.; Hu, Y.-S.; McFarland, E. W.; Hellman, A. Photoelectrochemical Hydrogen Production on  $\alpha\text{-Fe}_2\text{O}_3$  (0001): Insights from Theory and Experiments. *ChemSusChem* **2014**, *7*, 162–171.
- (28) Dotan, H.; Sivula, K.; Grätzel, M.; Rothschild, A.; Warren, S. C. Probing the Photoelectrochemical Properties of Hematite ( $\alpha\text{-Fe}_2\text{O}_3$ ) Electrodes Using Hydrogen Peroxide as a Hole Scavenger. *Energy Environ. Sci.* **2011**, *4*, 958–964.
- (29) Klahr, B. M.; Hamann, T. W. Current and Voltage Limiting Processes in Thin Film Hematite Electrodes. *J. Phys. Chem. C* **2011**, *115*, 8393–8399.
- (30) Shen, M.; Henderson, M. A. Identification of the Active Species in Photochemical Hole Scavenging Reactions of Methanol on  $\text{TiO}_2$ . *J. Phys. Chem. Lett.* **2011**, *2*, 2707–2710.
- (31) Panayotov, D. A.; Burrows, S. P.; Morris, J. R. Photooxidation Mechanism of Methanol on Rutile  $\text{TiO}_2$  Nanoparticles. *J. Phys. Chem. C* **2012**, *116*, 6623–6635.
- (32) Cummings, C. Y.; Marken, F.; Peter, L. M.; Tahir, A. A.; Wijayantha, K. G. U. Kinetics and Mechanism of Light-Driven Oxygen Evolution at Thin Film  $\alpha\text{-Fe}_2\text{O}_3$  Electrodes. *Chem. Commun.* **2012**, *48*, 2027–2029.
- (33) Braun, A.; Sivula, K.; Bora, D. K.; Zhu, J.; Zhang, L.; Grätzel, M.; Guo, J.; Constable, E. C. Direct Observation of Two Electron Holes in a Hematite Photoanode during Photoelectrochemical Water Splitting. *J. Phys. Chem. C* **2012**, *116*, 16870–16875.
- (34) Iandolo, B.; Hellman, A. The Role of Surface States in the Oxygen Evolution Reaction on Hematite. *Angew. Chem.* **2014**, *126*, 13622–13626.
- (35) Bertoluzzi, L.; Bisquert, J. Equivalent Circuit of Electrons and Holes in Thin Semiconductor Films for Photoelectrochemical Water Splitting Applications. *J. Phys. Chem. Lett.* **2012**, *3*, 2517–2522.
- (36) McDonald, K. J.; Choi, K. S. Photodeposition of Co-Based Oxygen Evolution Catalysts on  $\alpha\text{-Fe}_2\text{O}_3$  Photoanodes. *Chem. Mater.* **2011**, *23*, 1686–1693.
- (37) Le Formal, F.; Tetreault, N.; Cornuz, M.; Moehl, T.; Grätzel, M.; Sivula, K. Passivating Surface States on Water Splitting Hematite Photoanodes with Alumina Overlayers. *Chem. Sci.* **2011**, *2*, 737–743.
- (38) Cowan, A. J.; Barnett, C. J.; Pendlebury, S. R.; Barroso, M.; Sivula, K.; Grätzel, M.; Durrant, J. R.; Klug, D. R. Activation Energies for the Rate-Limiting Step in Water Photooxidation by Nanostructured  $\alpha\text{-Fe}_2\text{O}_3$  and  $\text{TiO}_2$ . *J. Am. Chem. Soc.* **2011**, *133*, 10134–10140.
- (39) Wang, X. G.; Weiss, W.; Shaikhutdinov, S. K.; Ritter, M.; Petersen, M.; Wagner, F.; Schlögl, R.; Scheffler, M. The Hematite ( $\alpha\text{-Fe}_2\text{O}_3$ ) (0001) Surface: Evidence for Domains of Distinct Chemistry. *Phys. Rev. Lett.* **1998**, *81*, 1038–1041.
- (40) Klahr, B.; Hamann, T. Water Oxidation on Hematite Photoelectrodes: Insight into the Nature of Surface States through In Situ Spectroelectrochemistry. *J. Phys. Chem. C* **2014**, *118*, 10393–10399.